Indian Journal of Geo Marine Sciences
Vol. 54 (10), October 2025, pp. 509-521
DOI: 10.56042/ijms.v54i10.18414

Research Article

An application of VNREDSat-1/NAOMI for Chlorophyll-*a* estimation

L Q Toan, C X Huy, N M Ngoc, L M Son, H Hai, B Q Huy, N P Hai & T T H Ai*

Vietnam National Space Center, Vietnam Academy of Science and Technology, 18 Hoang Quoc Viet, Nghia Do, Hanoi, Vietnam

*[E-mail: tthai@vnsc.org.vn, ai.tonghuyen@gmail.com]

Received 01 April 2025; revised 03 October 2025

Monitoring chlorophyll-*a* (Chl-*a*) concentrations using remote sensing techniques has been extensively studied across diverse marine and coastal environments. However, the optical complexity and dynamic nature of aquatic environments present significant challenges for such studies**.** This research aims to develop and evaluate two empirical models, a standard model (STD) and a calibration model (CAL), for estimating Chl-*a* content using VNREDSat-1 and Sentinel-2B images in the coastal estuary of Thua Thien Hue province, Vietnam. We used 29 paired datasets, comprising radiometric measurements and in-situ Chl-*a* samples, with 70 % for model development and 30 % for validation. The results indicate that the CAL model, which utilises spectral bands from the NAOMI sensor (VNREDSat-1) and MSI sensors (Sentinel-2B), estimates Chl-*a* concentration more effectively than the STD models, achieving R^2 values of 0.79 and 0.76, respectively. Furthermore, the RMSE, Bias, and MAE values of the CAL models are significantly lower than those of the STD models. Spatial analysis reveals that higher Chl-*a* concentrations are predominantly distributed in nearshore and shallow waters, whereas lower concentrations are observed in offshore and deeper waters. However, the study has several limitations, including a small sample size, challenges associated with atmospheric correction of VNREDSat-1 imagery, and difficulties in synchronising imagery with in-situ data. Further research is recommended to assess the potential of VNREDSat-1 data for water-quality monitoring in other coastal and estuarine environments in Vietnam.

[**Keywords**: Chl-*a* algorithms, Chlorophyll-*a* concentration, MSI sensor, NAOMI sensor, VNREDSat-1 images]

Introduction

Water quality monitoring is essential for protecting water resources and supporting environmental management for economic development and natural conservation[1]. Morel & Prieur[2] classified water into two categories: open ocean water, dominated by phytoplankton, and inland/coastal water, influenced by suspended matter and yellow substances. Coastal waters are highly productive ecosystems but are also vulnerable to environmental changes.

Spectral signals from the water surface, as detected by optical sensors, originate from the interaction of incident solar radiation with key water constituents, including suspended sediments, phytoplankton and Dissolved Organic Matter (DOM)[3,4]. Variations in these factors alter the spectral behaviour of the water body. In ocean colour studies, phytoplankton is the primary factor affecting water colour[5]. Chlorophyll is a key parameter in the photosynthesis process of phytoplankton[6-7]. Chlorophyll-*a* (Chl-*a*) is the most abundant of the chlorophylls (*a*, *b*, *c*, and *d*) and found in all algae[8]. Its concentration helps detect algal blooms[9] and estimate primary productivity[10], making it a crucial indicator of aquatic trophic status[7,8,11].

Based on literature reviews, Chl-*a* can be measured using traditional on-site or laboratory analysis, which is effective but lacks spatial and temporal coverage for water quality monitoring[12]. Advances in remote sensing technology have led researchers to estimate Chl-*a* based on its stronger absorption in blue and red light compared to green[13,14]. Ocean colour satellites, such as Landsat sensors, have been used to estimate ocean environmental parameters. While useful for mapping bottom types in shallow waters[15], these sensors face limitations in studying phytoplankton concentrations due to radiometric, geometric, revisit, and data costs[16]. NASA's Coastal Zone Colour Scanner (CZCS) aboard the Nimbus-7 environmental satellite was the first to observe Chl-*a*[17]. These data have opened a new perspective on monitoring ocean biochemical processes, colour and temperature, particularly in coastal zones[5,16].

With the growing diversity of satellite imagery, Chl-*a* retrieval algorithms have undergone continuous refinement. Most methods rely on empirical relationships between in-situ spectral reflectance and those extracted from imagery[4]. Morel & Prieur[2] developed a reflectance ratio algorithm using the Blue

(440 nm) and Green (560 nm) wavelength ranges to estimate Chl-*a* in seawater. These wavelengths correspond to the maximum and minimum absorption values of plant pigments. This algorithm has been most successfully applied in open-ocean areas[7], where Chl-*a* concentrations are below 30 mg/m[(refs. 3,18)]. O'Reilly[6] expanded this approach by incorporating the Green band (550–555 nm) into the SeaWiFS-derived ocean colour series (OCx), comprising 65 empirical Chl-*a* algorithms. Chlorophyll-*a* has a peak absorption at 443 nm (a wavelength available on most ocean colour sensors), but stronger absorption occurs at 412 nm[(ref. 19)]). Consequently, sensors with spectral channels below 443 nm (such as 412 nm) may be beneficial for detecting chlorophyll under certain conditions. Sentinel-2 Multispectral Images (MSI), despite being originally designed for land studies, have also demonstrated success in water applications due to their narrow spectral range in the Blue region (443 nm)[20]. In coastal regions, researchers have used MSI data to evaluate Chl-*a* distribution at the water surface using OCx algorithms, such as OC2 in the Bay of Bengal (Thailand)[21] and OC3 in Gabes Bay (Tunisia)[22], Chesapeake Bay[23], and the Barents Sea[24]. Additionally, the National Aeronautics and Space Administration (NASA) has applied these algorithms to generate an ocean-wide Chl-*a* map, achieving retrievals above 0.35 mg/m^3[(ref. 25)].

With its important geographical position, Chl-*a* content in Vietnamese waters has been studied using various satellite imagery sources, such as MODIS in Tien Yen Bay (Northern Vietnam Sea)[26], the integration of MODIS, Landsat ETM, ALOS and AVNIR-2[(ref. 27)], as well as OLCI data[28] for the Southern Centre of Vietnam coastal. Additionally, MERIS data have been used for studies covering the entire Vietnamese coastal region[29]. These studies employed different Chl-*a* models; however, all relied on ratio-based algorithms using the Blue and Green bands. For example, Ha *et al.*[26] proposed a Green/Blue model utilising the 551 nm and 443 nm bands of MODIS/Terre images to account for the Chl-*a*'s biooptical properties. Tong *et al.*[27] applied OC3 to images with varying spatial resolutions to determine the period, location, and morphology of algal blooms. Meanwhile, Binh *et al.*[28] and Loisel *et al.*[29] demonstrated that OC5 provides the highest accuracy in estimating Chl-*a*. These studies have highlighted the strong potential of using multi-temporal remote sensing for Chl-*a* extraction in Vietnam's coastal areas[28]. However, no research has yet explored VNREDSat-1 imagery to estimate Chl-*a* content in Vietnamese waters.

VNREDSat-1 is Vietnam's first multispectral optical satellite, designed for resource management, environmental monitoring, and disaster management[30]. Successfully launched on May 7, 2013, the satellite is equipped with the NAOMI (New AstroSat Optical Modular Instrument) sensor, which includes four multispectral bands (10 m resolution) and one panchromatic band (2.5 m resolution)[31,32]. While this sensor was originally intended for land cover mapping and related applications[33], VNREDSat-1 has also been used for marine studies, including research in the Truong Sa islands[34], bathymetry mapping along the Ninh Hai coast[35], and Suspended Particulate Matter (SPM) mapping in Vietnam's coastal waters[32]. However, these studies have not specifically focused on applying VNREDSat-1 imagery to extract Chl-*a* content in Vietnam's coastal areas.

This study aims to estimate Chl-*a* concentrations using appropriate empirical algorithms for Sentinel-2 and VNREDSat-1 in Thua Thien Hue's coastal area. Based on the correlation between in-situ Chl-*a* and spectral reflectance measurements, previously developed OC2-3 algorithms will be adjusted to fit MSI and VNREDSat-1 bands. The findings of this study can provide valuable information to support local authorities and environmental management agencies in developing effective strategies to protect and conserve marine resources.

Materials and Methods

Study area

The study area is the Thuan An coastal estuary in Thua Thien Hue province, with a 120 km-long coastline[36] (Fig. 1). The interaction between the rivers and the marine environment (seas) creates a highly diverse and dynamic estuarine ecosystem. The region hosts up to 416 phytoplankton species[36], with the lagoon alone containing 357 species[37]. Variations in salinity, turbidity, temperature, and suspended or dissolved materials create differences in phytoplankton concentrations between the lagoon and coastal waters. Additionally, these factors fluctuate seasonally due to influences from tides, wind, waves, and coastal currents.

The water quality characteristics in the Thuan An estuarine coastal and lagoon exhibit pronounced

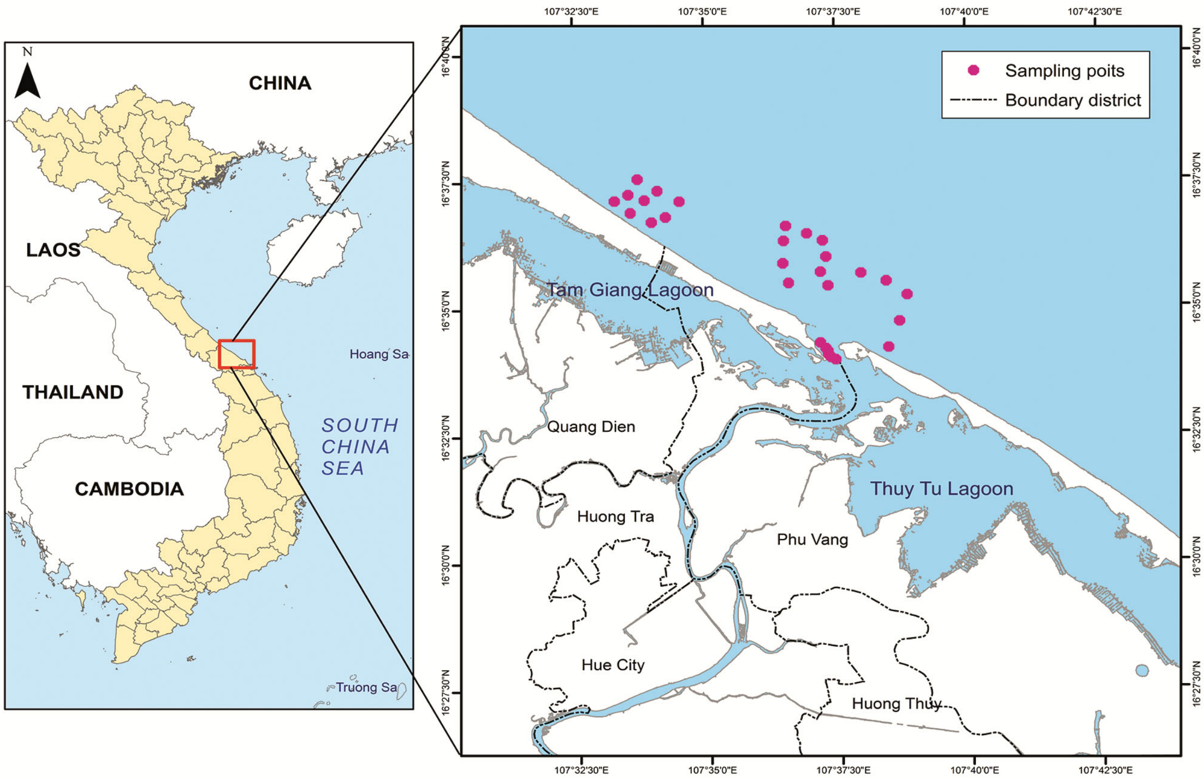

Fig. 1 — Location of the study area

Table 1 — Observation data

Number of samples	Detpth (m)	Chl-*a* (mg/m^3)			SPM (mg/m^3)		
		Min	Max	Mean	Min	Max	Mean
14	< 10	1.10	5.81	2.63	5.6	10.3	8.26
7	10–20	1.01	2.45	1.65	4.9	7.9	6.36
8	> 20	0.95	2.19	1.63	3.9	8.3	5.97
Total: 29	13.45	0.95	5.81	2.08	3.9	10.3	7.17

seasonal variations. Dissolved Oxygen (DO), Chemical Oxygen Demand (COD), and Biochemical Oxygen Demand (BOD) in the lagoon are higher than in the coastal area. Particularly during the rainy season, river flows carriesmore sediments, sand, and suspended matter, significantly increasing turbidity. During the dry season, the lagoon's water level is lower than the adjacent coastal at high-tide, leading to significantly decrease in salinity. The average turbidity in the lagoon is 20 mg/m^3, which is approximately 5 mg/m^3 higher than that of the coastal area. Consequently, the water at Thuan An estuarine is relatively clear, with low turbidity and fewer phytoplankton compared to the Tam Giang-Cau Hai lagoon.

Data use

We collected 29 in-situ samples between April 8th and April 13th, 2022, under clear and cloud-free weather conditions. These points were distributed along the Thua Thien Hue's coastal estuary, with an average depth of 13.45 m (Fig. 1). At each site, we recorded water surface radiance using a TriOS RAMSES radiometer and collected depth measurements and biogeochemical data. Laboratory analysis focused on Chl-*a* (mg/m^3) and SPM (mg/m^3) concentration.

Table 1 presents the statistical results of Chl-*a* and SPM concentrations across different depths. The average Chl-*a* and SPM concentrations were 2.08 mg/m^3 and 7.17 mg/m^3, respectively. Chl-*a* concentration decreases with increasing depth. At a depth < 10 m, the maximum Chl-*a* and SPM values were 5.81 mg/m^3, 10.3 mg/m^3, respectively. In deeper areas (> 20 m), both Chl-*a* and SPM concentrations were lower. This indicates an inverse relationship between Chl-*a*/SPM and water depth in the Thua

Thien Hue coastal. These field data are used for model development and validation[4].

The spectral reflectance of the water surface (Rrs) was measured using a TriOS radiometer with a 1 nm spectral resolution over the wavelength range of 380–1141 nm[ref. 38]. The sampling positions were recorded simultaneously using a GPS device. The data were collected, radiometrically calibrated using nominal calibration constants, and exported to Microsoft Excel for processing.

For model development and validation, the in-situ radiometric and biogeochemical data were divided into two subsets: 70 % (n = 20) for model development and 30 % (n = 9) for validation. The model input included only VNREDSat-1- and Sentinel-2B-simulated Rrs values in the 440–600 nm range. Hyperspectral Rrs values were convolved to match the satellite sensor bands: 485 nm and 565 nm for VNREDSat-1; and 442 nm, 492 nm, and 559 nm for MSI-2B. At each in-situ sample, a single Rrs spectrum was adjusted according to the hyperspectral weight of each image band[32], as provided by the satellite manufacturer in the spectral response function documentation.

For satellite data, we used two VNREDSat-1 images acquired on April 8 and April 13, 2022, and one Sentinel-2B image acquired on April 10, 2022. All images were obtained at Level-1 processing and contain Top-Of-Atmosphere (TOA) radiance values. The spectral and spatial resolution characteristics of these datasets are summarised in Table 2. Sentinel-2B multispectral imagery (MSI-2B) consists of 13 spectral bands covering the visible to shortwave infrared regions[39], with spatial resolutions of 10 m, 20 m, and 60 m, making it well-suited for coastal studies[21,22]. VNREDSat-1 imagery includes four spectral bands in the visible and near-infrared range[31], all with a spatial resolution of 10 m, comparable to the 10 m bands of Sentinel-2B.

These cloud-free level 1 images underwent pre-processing, including atmospheric and geometric correction. Ngoc *et al.*[31] introduced a RED-NIR algorithm for atmospheric correction of VNREDSat-1 imagery in clear to moderately turbid waters. This method applies to sensors without SWIR bands by using the relationship between NIR and visible wavelengths, following principles used in atmospheric correction for the POLDER instrument (on board the ADEOS-2 satellite) and the Geostationary Ocean Colour Imager (GOCI). In this study, the authors applied the RED-NIR algorithm to both images for atmospheric correction.

Table 2 — Spectral bands and spatial resolution of VNREDSat-1 and Sentinel-2B

Bands	VNREDSat-1		Sentinel-2B	
	Central wavelength (nm)	Resolution (m)	Central wavelength (nm)	Resolution (m)
Blue	485	10	492.1	10
Green	565	10	559.0	10
Red	655	10	664.9	10
Nir	825	10	832.9	10
Red edge 1			703.8	20
Red edge 2			739.1	20
Red edge 3			779.7	20
Red edge 4			864.0	20
Swir 1			1610.4	20
Swir 2			2185.7	20
Aerosols			442.2	60
Water vapour			943.2	60
Cirrus			1376.9	60

Empirical algorithm

Most remote sensing-derived Chl-*a* algorithms are based on an empirical relationship between spectral bands or ratio bands and in-situ Chl-*a* measurements[4]. O'Reilly & Werdell[19] developed the OCx algorithms to extract Chl-*a* from remote sensing images in regions where Chl-*a* concentrations exceed 0.35 mg/m^3. Among these, the OC2 and OC3 algorithms are widely used by NASA for global ocean Chl-*a* mapping[25].

To determine suitable empirical coefficients for OC2 and OC3 for VNREDSat-1 and Sentinel-2B images, current study implemented these algorithms using two approaches: the standard (STD) and calibration (CAL) models. The STD model directly applies published coefficients derived from POLDER-2 imagery[19]. To develop OCx_CAL models, we assessed the correlation between 20 paired in-situ Chl-*a* concentrations and spectral reflectance values (Rrs(λ)) obtained from the TriOS instrument. The Rrs(λ)_TriOS values were selected based on the central wavelengths corresponding to VNREDSat-1 (485 nm, 565 nm) and Sentinel-2B (442 nm, 492 nm, 559 nm). This empirical model is then applied to estimate Chl-*a* concentrations from VNREDSat-1 and Sentinel-2B images in the study area. The workflow diagram is shown in Figure 2.

The OC2 algorithm, one of NASA's earliest Chl-*a* retrieval methods, utilises the ratio of reflectance at

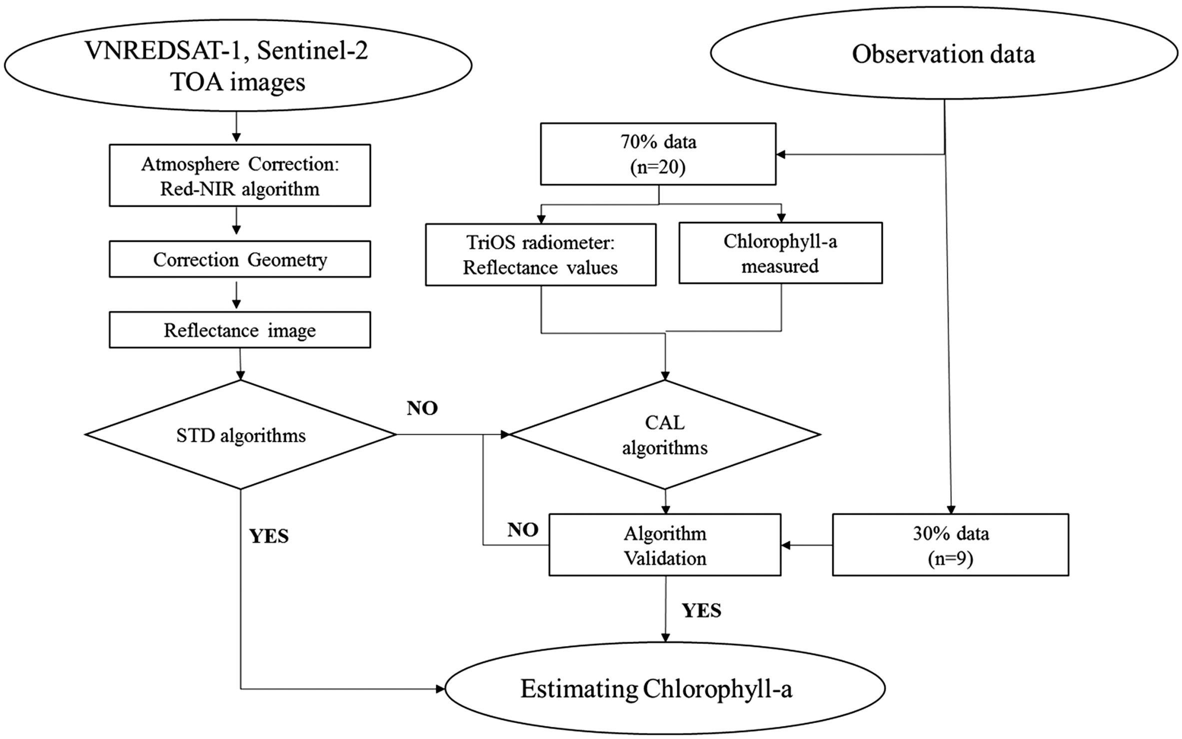

Fig. 2 — Workflow diagram for estimating chlorophyll-*a* (Chl-*a*) concentration using VNREDSat-1 and Sentinel-2 satellite imagery combined with in situ measurements

Table 3 — The OC2 and OC3 algorithms utilize band ratios (R) and polynomial coefficients (ao-a4) for Equation (1), respectively

Sensor	Algorithms	R	a0	a1	a2	a3	a4
POLDER-2	OC2_STD	$\log_{10}\left(\frac{443}{565}\right)$	0.19868	-1.78301	0.84573	0.19455	-0.95628
POLDER-2	OC2_STD	$\log_{10}\left(\frac{490}{565}\right)$	0.19868	-1.78301	0.84573	0.19455	-0.95628
VNREDSat_1	OC2_CAL	$\log_{10}\left(\frac{485}{565}\right)$	0.1854	0.5886	-3.1071	2.7671	0.1148
POLDER-2	OC2_STD	$\log_{10}\left(\frac{443}{565}\right)$	0.19868	-1.78301	0.84573	0.19455	-0.95628
POLDER-2	OC3_STD	$\log_{10}[\max\left(\frac{443}{565},\frac{490}{565}\right)]$	0.41712	-2.56402	1.22219	1.02751	-1.56804
Sentinel-2B	OC2_CAL	$\log_{10}\left(\frac{442}{559}\right)$	0.1504	0.5672	-2.9671	2.7182	0.0177
Sentinel-2B	OC3_CAL	$\log_{10}[\max\left(\frac{442}{559},\frac{492}{559}\right)]$	0.3371	-0.3309	0.1664	-0.0477	-0.1385

443 nm and 565 nm(ref. 19). The OC3 algorithm extends OC2 by incorporating an additional green band, using the maximum ratio between reflectance at 443 nm and 490 nm relative to 565 nm. These OCx algorithms were logarithmically transformed[40], and empirical coefficients for Chl-*a* retrieval were derived through fitting a fourth-order polynomial function[19]. VNREDSat-1 image without the 490 nm band, only the OC2 algorithm can be applied. Sentinel-2B provides the appropriate bands for the implementation of both OC2 and OC3 algorithms. The general OCx formulation[19] is expressed as:

$$OCx = 10^{(a0 + a1 \times R + a2 \times R^2 + a3 \times R^3 + a4 \times R^4)} \quad \ldots (1)$$

The empirical coefficients (a_0–a_4) and their corresponding R-ratio bands vary depending on the sensor type. Detailed values of these coefficients are presented in Table 3.

Table 4 — Statistic metrics between Chl-*a* estimation and Chl-*a* observation

Satellite	Algorithms	R^2	RMSE	Bias	MAE
VNREDSat_1	OC2_STD with R= $\log_{10}\left(\frac{443}{565}\right)$	0.2546	2.2565	1.9532	0.9999
	OC2_STD with R= $\log_{10}\left(\frac{490}{565}\right)$	0.3249	1.8272	1.2559	1.1020
	OC2_CAL with R=$\log_{10}\left(\frac{485}{565}\right)$	0.7935	1.2083	0.3812	0.3214
Sentinel-2B	OC2_STD with R= $\log_{10}\left(\frac{443}{565}\right)$	0.3769	1.219	0.5493	0.2788
	OC3_STD with R= $\log_{10}[\max\left(\frac{443}{565},\frac{490}{565}\right)]$	0.2596	1.7979	1.2093	1.0694
	OC2_CAL with R =$\log_{10}\left(\frac{442}{559}\right)$	0.6968	1.2934	0.5987	0.3069
	OC3_CAL with R= $\log_{10}[\max\left(\frac{442}{559},\frac{492}{559}\right)]$	0.7696	1.1551	0.2741	0.4729

Evaluation of Chl-*a* models

The accuracy of Chl-*a* estimation models from satellite images (Ei) is assessed by comparing them with in-situ Chl-*a* measurements (Mi), using four statistical indices: coefficient of determination (R^2), Root Mean Square Error (RMSE), Mean Absolute Error (MAE), and Bias. Model validation is conducted using an independent in-situ dataset (n = 9). The statistical metrics are calculated as follows:

$$R^2 = \frac{\left(\sum(E_i-\bar{E})(M_i-\bar{M})\right)^2}{\sum(E_i-\bar{E})^2\sum(M_i-\bar{M})^2} \quad \text{... (2)}$$

$$RMSE = \left[\frac{\sum_{i=1}^{N}(\log_{10}E_i-\log_{10}M_i)^2}{n}\right]^{1/2} \quad \text{... (3)}$$

$$MAE = \frac{1}{n} * \sum_{i=1}^{N}\frac{|\log_{10}E_i-\log_{10}M_i|}{|\log_{10}E_i|} \quad \text{... (4)}$$

$$Bias = [\sum_{i=1}^{n}(\log_{10}E_i - \log_{10}M_i)/n] \quad \text{... (5)}$$

All statistical metrics are computed using log10-transformed Chl-*a* concentrations, as Chl-*a* distribution follows an approximately log-normal pattern[41]. This transformation enhances the coefficient of determination (R^2)[19,24].

R^2 measures how well the model fits the in-situ data. A value close to 1 indicates a strong correlation and better model performance. RMSE reflects the average deviation between estimated and measured Chl-*a* values (mg/m^3). A lower RMSE (~ 0) indicates higher accuracy. MAE measures the absolute difference between satellite-derived and in-situ Chl-*a* values. A smaller MAE indicates better agreement between the two datasets. Bias represents systematic errors in model predictions (mg/m^3), a value near zero indicates minimal consistent over- or underestimation. The highest R^2 and the lowest RMSE, Bias and MAE determine the optimal Chl-*a* estimation model.

Results

Accuracy assessment

The statistical metrics comparing the 9 paired Chl-*a* values derived from models with in-situ Chl-*a* measurements are presented in Table 4. The results indicate that the CAL model consistently outperforms the STD model across all statistical metrics. Specifically, the CAL model achieved a higher R^2 value than the STD model, demonstrating a significantly stronger correlation with the in-situ observation. Additionally, the lower RMSE, Bias and MAE of CAL reflect reduced estimation errors and improved accuracy. These findings confirm that the CAL model provides better Chl-*a* estimates than the STD model**.**

As illustrated in Figure 3, the Chl-*a* distribution based on the CAL model is more consistent with Chl-*a* in-situ than the STD model. For VNREDSat-1 imagery, the 443/565 nm-based STD algorithm underestimated Chl-*a*. The 490/565 nm-STD leads to overestimated values. The 485/565 nm ratio in the CAL model yields more accurate results compared to the STD model. For Sentinel-2B, the scatter plots show that CAL approaches are more consistent across different band ratios than the STD model.

The STD model is ineffective for both VNREDSat-1 and MSI-2B spectral data in the study area. R^2 values remain below 0.4, indicating a weak correlation with Chl-*a* in-situ. The statistical parameters in Table 4 confirm that the experimental coefficients of the STD model are not suitable for estimating Chl-*a* in the Thua Thien Hue's coastal area. The CAL model significantly improves Chl-*a*

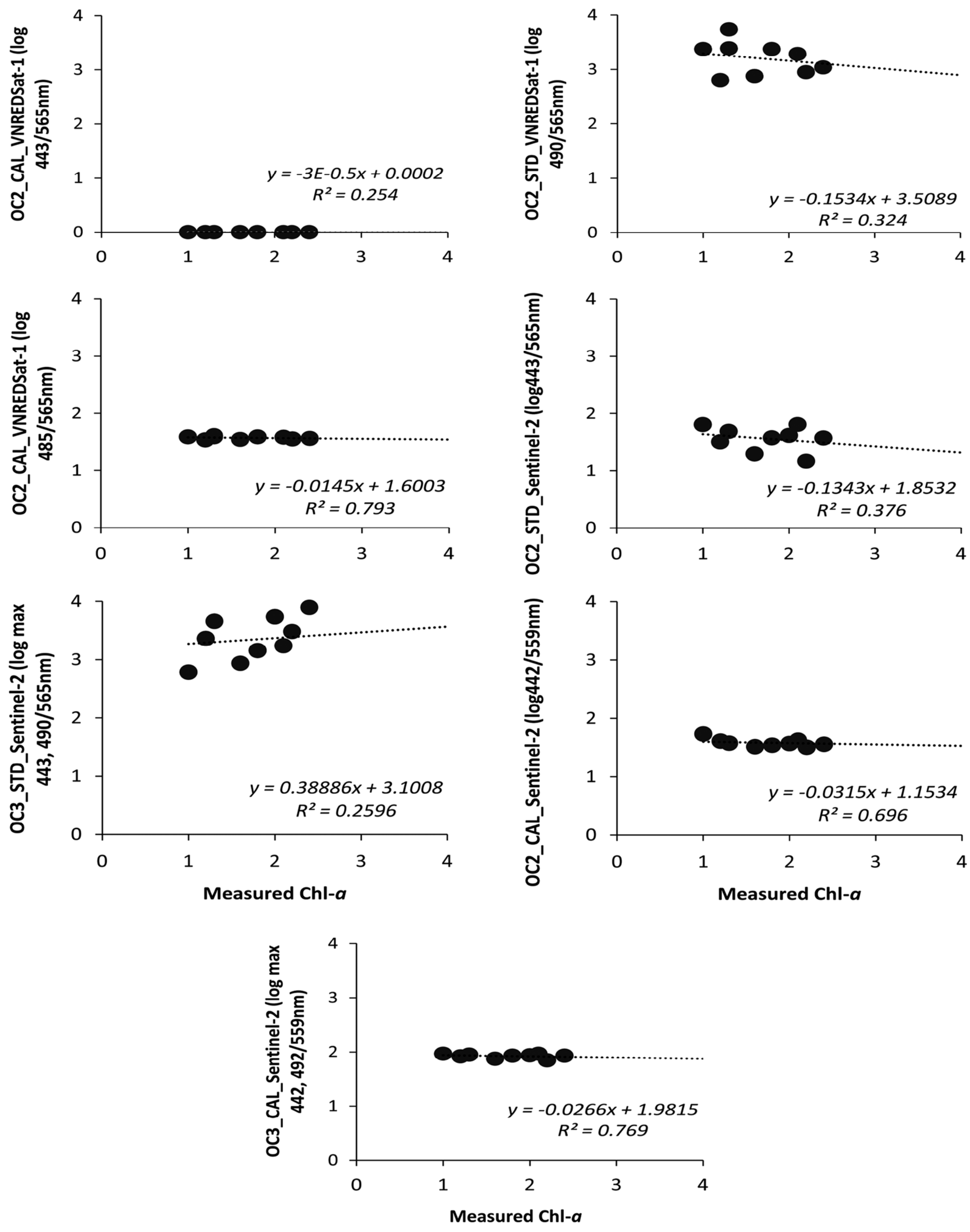

Fig. 3 — Accuracy plots for Chl-*a* retrievals from VNREDSat-1/Sentinel-2 and Chl-*a* in situ

estimation accuracy and should be preferred over the STD model for this study area.

The CAL model significantly improves Chl-*a* retrieval accuracy by utilising the original image wavelengths. For VNREDSat-1 data, the R^2 value increases from 0.2546 to 0.7935, while RMSE decreases from 2.2565 to 1.2083. In addition, the Bias and MAE are notably reduced to 0.3812 and 0.3124, respectively. Similar improvements are observed for the Sentinel-2B sensor. For the OC3 model, the R^2 value advances significantly from 0.2596 to 0.7696, whereas for OC2 model it increases from 0.3769 to 0.6968. Moreover, the Bias-based OC3 is remarkably low at 0.2741. In all cases, the CAL model consistently outperforms the STD model, providing more reliable estimates of Chl-*a* concentrations. Therefore, these CAL algorithms are applied to generate Chl-*a* maps derived from VNREDSat-1 and MSI-2B for the study area.

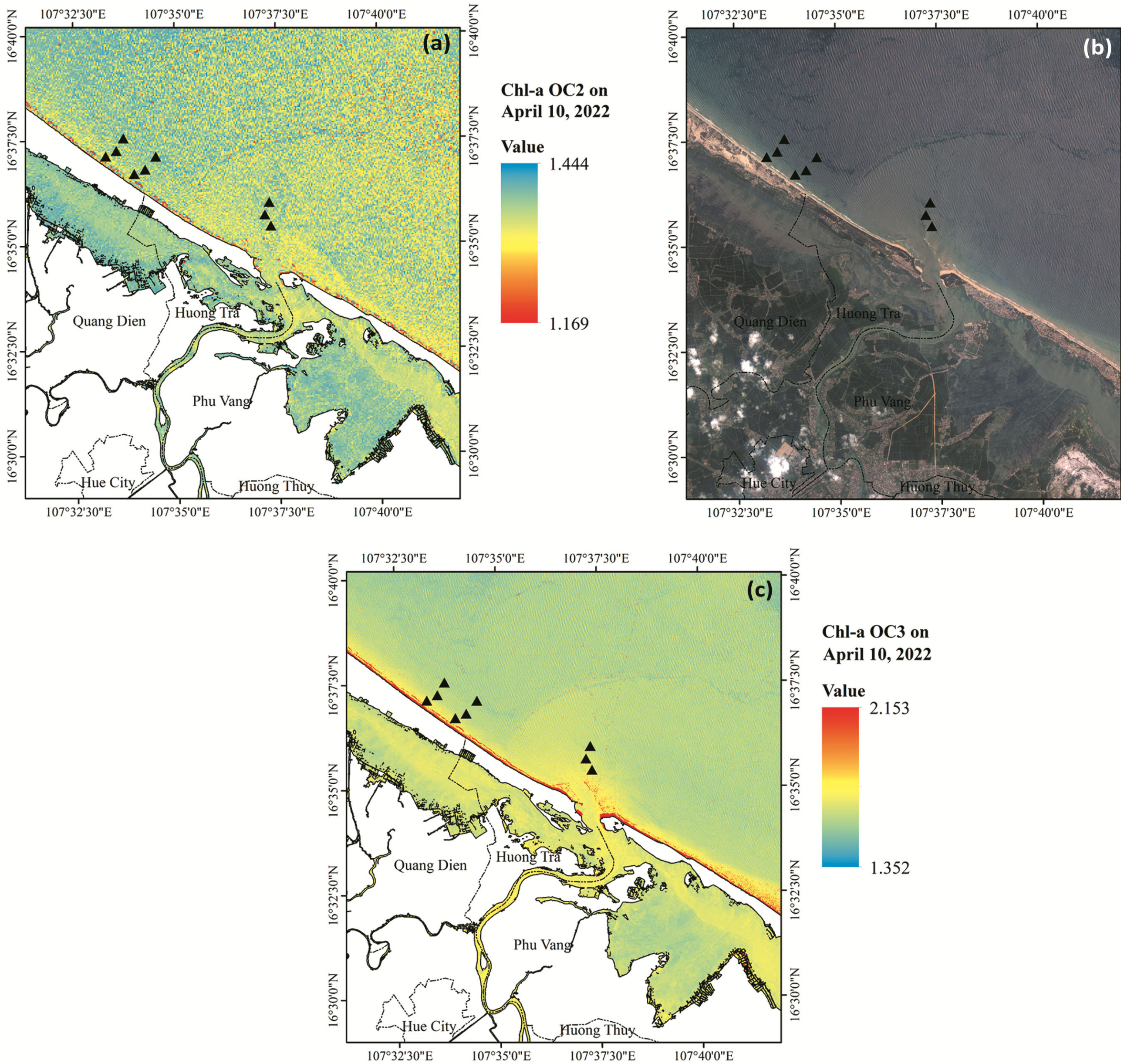

Fig. 4 — Chl-*a* maps using CAL model and Sentinel-2B L1 true colour on April 10th, 2022: a) OC2-CAL; b) Sentinel-2B L1; and c) OC3-CAL

Chl-*a* mapping

The OC2 and OC3 algorithms were applied to generate Chl-*a* maps from Sentinel-2B and VNREDSat-1 images for the study area's coastal region. The reliability of these models was assessed by comparing the estimated Chl-*a* concentrations with in-situ measurements.

Figure 4 illustrates Sentinel-2B-derived Chl-*a* maps on April 10th, 2022, using cloud-free images. The different algorithms produced distinct spatial distributions of Chl-*a* concentrations. OC2 estimated Chl-*a* values ranging from 1.169 to 1.444 mg/m^3. OC3 produced higher Chl-*a* from 1.352 to 2.153 mg/m^3. The average field-measured Chl-*a* value at the marked positions was 1.57 mg/m^3 (Table 5). When comparing these estimates with in-situ data,the OC2-derived Chl-*a* values (1.37 mg/m^3) were closer with the observed values. OC3-derived Chl-*a* estimates (2.08 mg/m^3) were noticeably higher. The spatial distribution of Chl-*a* concentrations is clearly illustrate in the map, with colours gradient shifting from light blue to orange, corresponding to the transition from offshore waters to nearshore areas. Higher Chl-*a* concentrations (orange) are observed in the nearshore area, whereas lower values (light blue) are found farther offshore.

Table 5 — Mean Chl-*a* estimated from CAL model at marked locations

Detpth (m)	Chl-*a* in-situ (mg/m^3)	Sentinel-2B_ CAL		VNREDSat-1_CAL	
		OC2	OC3	April 08, 2022	April 13, 2022
< 10	1.61	1.41	2.09	1.35	1.59
10–20	1.63	1.45	2.11	1.36	1.58
> 20	1.50	1.24	2.04	1.31	1.55
Average	1.57	1.37	2.08	1.34	1.57

Additionally, the Chl-*a* maps generated using the CAL model from two VNREDSat-1 scenes acquired on April 8th and 13th, 2022 are shown in Figure 5. This model provides Chl-*a* content from 1.113 to 1.663 mg/m^3 (for April 13th) and 0.006 to 1.594 mg/m^3 (for April 8th). At the marked locations, the estimated Chl-*a* values for both acquisition dates are slightly closer to the in-situ measurement. Similar to the MSI-2B-extracted Chl-*a* map, higher Chl-*a* concentrations (orange) is observed in the nearshore region, whereas lower concentrations (light blue) are distributed farther offshore. These results confirm that the CAL model effectively captures the spatial variability of Chl-*a*

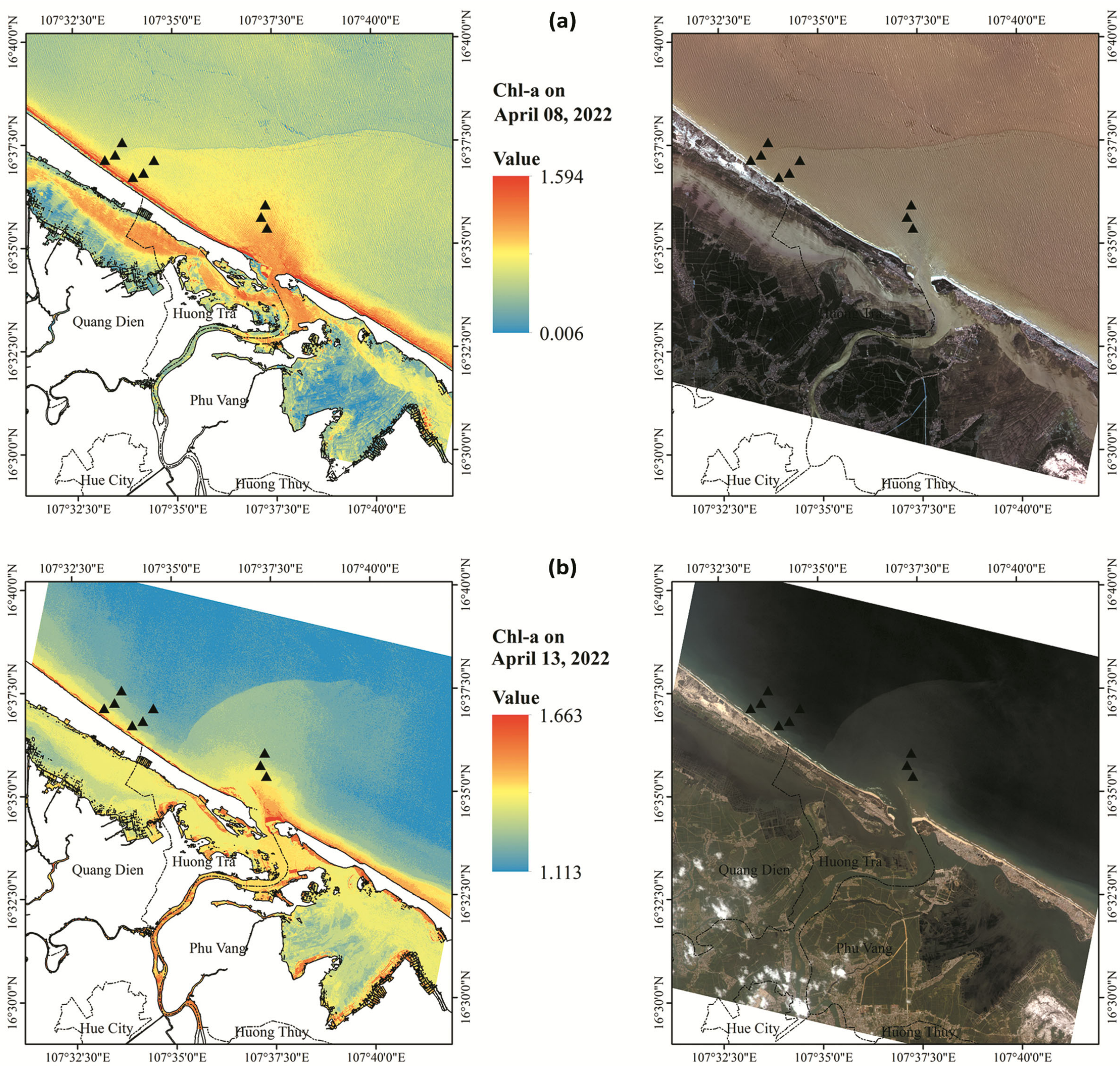

Fig. 5 — Chl-*a* maps using OC2-CAL model and VNREDSat-1 L1 true color: a) April 8th, 2022; and b) April 13th, 2022

distribution, making it a reliable approach for monitoring coastal water quality.

The in-situ analysis in the previous section revealed that Chl-*a* concentrations were lower in deep water than in shallow areas**.** To validate this pattern, the estimated Chl-*a* concentrations at marked locations were analysed with different depths, as summarised in Table 5**.** The results confirm that Chl-*a* retrieved from MSI-2B and VNREDSat-1 follow spatial distribution pattern similar to that of the field measurements. Specifically, in shallow waters (< 10 m depth)**,** the OC2_MSI-2B algorithm estimates a Chl-*a* at 1.41 mg/m^3. At depths > 20 m, this value decreases to 1.24 mg/m^3, whereas the average in-situ Chl-*a* concentration is 1.37 mg/m^3. Regarding the CAL model, the average VNREDSat-1-derived Chl-*a* value (April 13th, 2022) matches the measured concentration of 1.57 mg/m³ exactly. The April 8th, 2022 VNREDSat-1-derived Chl-*a* is also highly consistent with in-situ Chl-*a* at 1.34 mg/m^3. For the Sentinel-2B imagery**,** the OC2 algorithm produced an estimate (1.37 mg/m^3) that better agreement with observed data than the OC3**,** which yielded a higher values of 2.08 mg/m^3. Although Chl-*a* values retrieved by OC3 at marked locations exceed 2 mg/m^3, they still fall within the general range of *in situ* Chl-*a*. These analyses confirm that the CAL model, when applied to VNREDSat-1 and Sentinel-2B images, provides reliable Chl-*a* products.

Discussion

In addition to Chl-a**,** we also measured Suspended Particulate Matter (SPM) to analyse the relationship between Chl-*a* and other aquatic environmental factors (Table 1). Despite the study area being an estuary with aquaculture lagoons, in-situ data indicate low concentrations of both Chl-*a* (7.17 mg/l) and SPM (2.08 µg/l). This suggests that Thua Thien Hue's coastal waters remain relatively clear during the dry season (April, 2022). These conditions justify the use of the RED/NIR-based atmospheric correction algorithm for VNREDSat-1 imagery, as this method has been demonstrated to be effective for clear to moderately turbid waters on the NAOMI sensor[31]. Accordingly, the use of the RED/NIR algorithm for atmospheric correction in this study is considered appropriate.

In estuarine areas, sediment load increases during the rainy season, resulting in higher turbidity and posing greater challenges for atmospheric correction. Currently, there are very few studies addressing atmospheric correction for VNREDSat-1 imagery, particularly under turbid water conditions. Atmospheric correction is a critical factor in Chl-*a* retrieval[16], and multiple algorithms have been developed, including SeaDAS, ACOLITE, C2RCC, POLYMER, Sen2Cor, I2gen, and iCOR[(refs. 7,23,42,43)]. However, each method has limitations: C2RCC struggles with coastline pixels[7], POLYMER is less effective in highly eutrophic waters[23], and Sen2Cor and iCOR perform ineffectively in coastal environments[42]. There is no universal atmospheric correction method applicable to all satellite sensors[42], and each region presents unique challenges[43]. Although the RED/NIR algorithm is suitable for VNREDSat-1 imagery in clear to moderately turbid waters[31], its effectiveness in estuaries remains challenging. Additionally, as this study employed the same atmospheric correction method for both NAOMI and MSI-2B sensors**,**, the CAL model still contains uncertainties**.** Furthermore, the limited spectral coverage of VNREDSat-1 present significant challenges for accurate atmospheric correction in coastal regions. Therefore, these issues require further research[40].

Vietnam has a tropical monsoon climate resulting in coastal region are frequently affected by persistent cloud cover[28]. In particular, the Thua Thien Hue rarely yields cloud-free VNREDSat-1 imagery. To enhance temporal coverage for Chl-*a* monitoring, integrating multiple remote sensing data sources with comparable spectral characteristics, such as Sentinel-2, is essential. In this study, Sentinel-2B imagery is used to compensate for the limited availability of cloud-free VNREDSat-1 data because it is freely available and provides a spatial resolution comparable to that of VNREDSat-1 to. The STD and CAL models were implemented to estimate Chl-*a* from Rrs derived from VNREDSat-1 and Sentinel-2B images. The model estimates are subsequently validated against in-situ data. The results demonstrated that the CAL model outperforms the STD method, achieving ahigher R^2 values and significantly lower RMSE, Bias and MAE values. These findings confirm the effectiveness of the CAL model for accurate estimation of Chl-*a* concentrations in coastal waters.

In coastal studies, theaccuracy of Chl-*a* retrieval algorithm is influenced by several factors, including the spatial distribution of sampling sites, collection time of field data, and uncertainty associated with in-situ data[24]. To minimise seasonal variability and enhance model reliability, observed data were collected during the dry season. Moreover, this dataset was spatially distributed across both estuarine and coastal regions to ensure environmental representativeness for the study area. Model performance was evaluated using RMSE, MAE, and sample size, all of which are critical factors in determining model accuracy and associated uncertainty. A larger sample size generally increases the statistical power to detect reliable patterns. In this study, 29 samples were collected, of which 20 were used for model development and 9 for validation. This relatively small sample size is a limitation of the study. However, Curran & Williamson[44] suggested that, with 95 % confidence, a sample size between 1 and 58 may be sufficient for ground radiometric and airborne multispectral scanner measurements. In addition, Andrius Vabalas *et al.*[45] demonstrated that a strict separation between training and test datasets can yield objective performance estimates, regardless of sample size. Therefore, increasing the number of samples, particularly within aquaculture areas of the study region, is essential to improve the model's performance further.

Estimating Chl-*a* in coastal waters is challenging due to complex optical properties[16]. In Case 1 waters, where phytoplankton dominates color[40], the blue/green band-ratio algorithm is highly effective, as phytoplankton absorbs more blue light than green. In Case 2 waters, optical properties are influenced by multiple constituents, including chlorophyll, Colored Dissolved Organic Matter (CDOM) and Total Suspended Solids (TSS), which vary spatially and temporally. Therefore, band-ratio algorithms are less effective, and semi-analytical approaches may be more suitable[46]. During the rainy season, increased river discharge transports sediment and suspended matter into the Thua Thien Hue coastal areas[47], making Chl-*a* estimation difficult due to constantly changing water conditions[48]. The band-ratio bio-optical algorithm remains unreliable for this region. This study represents the first experimental evaluation of VNREDSat-1 imagery for Chl-*a* extraction in coastal water quality research. The findings highlight both the potential and challenges of using VNREDSat-1 for coastal monitoring, emphasising the need for further research on atmospheric correction and algorithm optimisation for turbid water conditions.

Conclusion

This study has demonstrated that the CAL model is effective in retrieving Chl-*a* concentrations from VNREDSat-1 and Sentinel-2B imagery in the coastal area of Thua Thien Hue during the dry season. The CAL model has a higher coefficient of determination (R^2) and lower RMSE, BIAS, and MAE values compared to the standard model (STD). Despite several remaining challenges such as synchronising imagery with in-situ data, weather conditions during data acquisition, atmospheric correction techniques, and a limited number of samples the CAL model has proven effective in mapping the spatial distribution of Chl-*a*. Higher Chl-*a* concentrations were observed in nearshore waters compared to offshore areas, and in shallow waters relative to deeper. These findings highlight the potential of VNREDSat-1 imagery for estimating Chl-*a* concentrations and other water quality parameters, emphasising the need for further research and application in other coastal environments.

Acknowledgements

This research utilised data provided by VAST under the project code QTRU.02.08/25-26, project name: "Research and application of marine survey data by the 9th OPARIN Academician ship and optical remote sensing/Radar image data in assessing the quality of water environment in the Central Coast of Vietnam".

Conflicts of Interest

The authors declare no conflict of interest.

Author Contributions

TTHA, LQT & NMN: Conceptualisation, formal analysis, and writing-original draft. CXH, LMS, BQH & HH: Data curation and software. TTHA & NPH: Investigation, validation, writing-review and editing. All authors have read and agreed to the published version of the manuscript.

References

1 Le C, Hu C, Cannizzaro J, English D, Muller-Karger F, *et al.*, Evaluation of Chlorophyll-a Remote Sensing Algorithms for an Optically Complex Estuary, *Remote Sens Environ*, 129 (2013) 75–89

2 Morel A & Prieur L, Analysis of variations in ocean color, *Limnol Oceanogr*, 22 (4) (1977) 709-722.

3 Gert A & Schult E T E, *Remote sensing in hydrology and water management*, (Springer), 2000, pp. 486.

4 Ritchie J C, Zimba P V & Everitt J H, Remote sensing techniques to assess water quality, *Photogramm Eng Remote Sens*, 69 (6) (2003) 695–704.

5 Dassenakis M, Paraskevopoulou V, Cartalis C, Adaktilou N & Katsiabani K, Remote sensing in coastal water monitoring: Applications in the eastern mediterranean sea (IUPAC technical report), *Pure Appl Chem*, 84 (2) (2012) 335–375.

6 O'Reilly J E, Maritorena S, Mitchell B G, Siegel D A & Carder K L, Ocean color chlorophyll algorithms for SeaWiFS, *J Geophys Res*, 103 (C11) (1998) 24937–24853.

7 Ansper A & Alikas K, Retrieval of chlorophyll a from Sentinel-2 MSI data for the European Union water framework directive reporting purposes, *Remote Sens*, 11 (1) (2019) 1-26 https://doi.org/10.3390/rs11010064

8 Aranha T R B T, Martinez J M, Souza E P, Barros M U G & Martins E S P R, Remote Analysis of the Chlorophyll-a Concentration Using Sentinel-2 MSI Images in a Semiarid Environment in Northeastern Brazil, *Water (Switzerland)*, 14 (3) (2022) p. 451. https://doi.org/10.3390/w14030451

9 Kutser T, Quantitative detection of chlorophyll in cyanobacterial blooms by satellite remote sensing, *Limnol Oceanogr*, 49 (6) (2004) 2179–2189.

10 Ross M R V, Topp S N, Appling A P, Yang X, Kuhn C, *et al*., AquaSat: A Data Set to Enable Remote Sensing of Water Quality for Inland Waters, *Water Resour Res*, 55 (11) (2019) 10012–10025.

11 Luoheng Han, Estimating chlorophyll-a concentration using first-derivative spectra in coastal water, *Int J Remote Sens*, 26 (23) (2005) 5235–5244.

12 Gregor J & Maršálek B, Freshwater phytoplankton quantification by chlorophyll a: a comparative study of in vitro, in vivo and in situ methods, *Water Res*, 38 (3) (2004) 517–522.

13 Charles S Y, The influence of phytoplankton pigments on the colour of sea water, *Deep Sea Res*, 7 (1) (1960) 1–9.

14 Gordon H R & Wang M, Retrieval of water-leaving radiance and aerosol optical thickness over the oceans with SeaWiFS: a preliminary algorithm, *Appl Opt*, 33 (3) (1994) 443-452.

15 Lyzenga D R, Remote sensing of bottom reflectance and water attenuation parameters in shallow water using aircraft and landsat data, *Int J Remote Sens*, 2 (1) (1981) 71–82.

16 Miller R L, Del Castillo C E & McKee B A, *Remote Sensing of Coastal Aquatic Environments: Technologies, techniques and applications*, (Remote Sensing and Digital Image Processing/Springer), 2007, pp. 357.

17 Acker J G, *The heritage of SeaWiFS: a retrospective on the CZCS NIMBUS Experiment Team (NET) program*, SeaWiFS Technical Report Series, NASA Technic/al Memorandum 104566, Vol 21, edited by Hooker S B & Firestone E R, (NASA Center for AeroSpace Information), 1994, pp. 47.

18 Schalles J F, Optical remote sensing techniques to estimate phytoplankton chlorophyll a concentrations in coastal waters with varying suspended matter and cdom concentrations, *Remote Sens Digit Image Process*, 9 (2006) 27–79.

19 O'Reilly J E & Werdell P J, Chlorophyll algorithms for ocean color sensors - OC4, OC5 & OC6, *Remote Sens Environ*, 229 (2019) 32–47.

20 Therese H E, Krause J D, Staehr P A, Brian G G & Boye H L, *Literature Review of Remote Sensing Technologies for Coastal Chlorophyll-a Observations and Vegetation Coverage*, Danish Centre for Environment and Energy, 2018, pp. 47.

21 Poddar S, Chacko N & Swain D, Estimation of Chlorophyll-a in Northern Coastal Bay of Bengal Using Landsat-8 OLI and Sentinel-2 MSI Sensors, *Front Mar Sci*, 6 (2019) 1-11. https://doi.org/10.3389/fmars.2019.00598

22 Katlane R, Dupouy C, El Kilani B & Berges J C, Estimation of Chlorophyll and Turbidity Using Sentinel 2A and EO1 Data in Kneiss Archipelago Gulf of Gabes, Tunisia, *Int J Geosci*, 11 (10) (2020) 708–728.

23 Pahlevan N, Smith B, Schalles J, Binding C, Cao Z, *et al*., Seamless retrievals of chlorophyll-a from Sentinel-2 (MSI) and Sentinel-3 (OLCI) in inland and coastal waters: A machine-learning approach, *Remote Sens Environ*, 240 (2020) p. 21.

24 Asim M, Brekke C, Mahmood A, Eltoft T & Reigstad M, Improving Chlorophyll-A Estimation from Sentinel-2 (MSI) in the Barents Sea Using Machine Learning, *IEEE J Sel Top Appl Earth Obs Remote Sens*, 14 (2021) 5529–5549.

25 Wang G, *Chlorophyll a (chlor_a)*, Accessed online at: https://oceancolor.gsfc.nasa.gov/resources/atbd/chlor_a/; (Accessed in 2023).

26 Ha N T T, Koike K & Nhuan M T, Improved accuracy of chlorophyll-a concentration estimates from MODIS Imagery using a two-band ratio algorithm and geostatistics: As applied to the monitoring of eutrophication processes over Tien Yen Bay (Northern Vietnam), *Remote Sens*, 6 (1) (2013) 421–442.

27 Son T P H, Chuan T M & Tin H C, Detecting Chlorophyll a Concentration and Bloom Patterns at Upwelling Area in South Central Vietnam by High Resolution Multi-satellite Data, *J Environ Sci Eng A*, 4 (5) (2015) 215-224.

28 Binh N A, Hoa P V, Thao G T P, Duan H D & Thu P M, Evaluation of Chlorophyll-a estimation using Sentinel 3 based on various algorithms in southern coastal Vietnam, *Int J Appl Earth Obs Geoinf*, 112 (2022) p. 11. https://doi.org/10.1016/j.jag.2022.102951

29 Hubert Loisel, Vantrepotte V, Ouillon S, Ngoc D D, Herrmann M, *et al*., Assessment and analysis of the chlorophyll-a concentration variability over the Vietnamese coastal waters from the MERIS ocean color sensor (2002–2012), *Remote Sens Environ*, 190 (2017) 217–232.

30 Chung D M, Space technology development in vietnam 2011-2012, In: *Proceedings of the Asia-Pacific Regional Space Agency Forum (APRSAF-19)*, Kuala Lumpur, Malaysia, 11–14 December 2012, pp. 14–17.

31 Ngoc D D, Loisel H, Duforêt-Gaurier L, Jamet C, Vantrepotte V, *et al*., Atmospheric correction algorithm over coastal and inland waters based on the red and NIR bands: application to Landsat-8/OLI and VNREDSat-1/NAOMI observations, *Opt Express*, 27 (22/28) (2019) 1-22.

32 Ngoc D D, Loisel H, Vantrepotte V, Xuan H C, Minh N N, *et al*., A simple empirical band-ratio algorithm to assess suspended particulate matter from remote sensing over coastal and inland waters of vietnam: Application to the VNREDSat-1/NAOMI sensor, *Water (Switzerland)*, 12 (9) (2020) p. 2326. https://doi.org/10.3390/w12092636

33 CEOS, *VNREDSat-1 MS Instrument*, Accessed online at: https://database.eohandbook.com/database/instrumentsummary.aspx?instrumentID=1681

34 Cuong D H, Anh B T B, Tung N X, Luan N T, Nam L D, *et al*., Application of satellite images and VNREDSAT-1 images in study on marine environment in Truong Sa region,

Vietnam J Mar Sci Technol, 19 (3B) (2019) 149–162. https://doi.org/10.15625/1859-3097/19/3B/14522

35 Van K L, Son T P H, Huan N H & Trung P B, Bathymetry mapping using VNREDSAT-1 image: A case study in Ninh Hai coast, Ninh Thuan province of Vietnam, *Vietnam J Mar Sci Technol*, 19 (4A) (2019) 67–77. https://doi.org/10.15625/ 1859-3097/19/4A/14605

36 People's Committee of Thua Thien Hue Province, *Geography of Thua Thien Hue – Natural Section*, (Science and Technology Publishing), 2005, pp. 307.

37 Viet Nam Environment Protection Agency, *Overview of Wetlands status in Viet Nam following 15 yeas of Ramsar convention implementation*, (Hanoi, Viet Nam), 2005, pp. 72.

38 Ruddick K G, Cauwer V De, Park Y J & Moore G, Seaborne measurements of near infrared water-leaving reflectance: The similarity spectrum for turbid waters, *Limnol Oceanogr*, 51 (2) (2006) 1167–1179.

39 Wang Q & Atkinson P M, Spatio-temporal fusion for daily Sentinel-2 images, *Remote Sens Environ*, 204 (2018) 31–42.

40 Gohin F, Druon J N & Lampert L, A five channel chlorophyll concentration algorithm applied to Sea WiFS data processed by SeaDAS in coastal waters, *Int J Remote Sens*, 23 (8) (2002) 1639–1661.

41 Neil C, Spyrakos E, Hunter P D & Tyler A N, A global approach for chlorophyll-a retrieval across optically complex inland waters based on optical water types, *Remote Sens Environ*, 229 (2019) 159–178.

42 Warren M A, Simis S G H, Martinez-Vicente V, Poser K, Bresciani M, *et al*., Assessment of atmospheric correction algorithms for the Sentinel-2A MultiSpectral Imager over coastal and inland waters, *Remote Sens Environ*, 225 (2019) 267–289.

43 Tian S, Guo H, Huang J J, Zhu X & Zhang Z, Comprehensive comparison performances of Landsat-8 atmospheric correction methods for inland and coastal waters, *Geocarto Int*, 37 (27) (2022) 15302–15323.

44 Curran P J & Williamson H D, Sampe size for ground and remotely sensed data, *Remote Sens Environ*, 20 (1) (1986) 31-41.

45 Andrius V, Gowen E, Poliakoff E & Alexcander J C, Machine learning algorithm validation with a limited sample size, *Plos One*, 14 (11) (2019) p. e0224365. https://doi.org/10.1371/journal.pone.0224365

46 Hu C, Chen Z, Clayton T D, Swarzenski P, Brock J C, *et al*., Assessment of estuarine water-quality indicators using MODIS medium-resolution bands: Initial results from Tampa Bay, FL, *Remote Sens Environ*, 93 (3) (2004) 423–441.

47 Geographical Gazetteer of Thua Thien Hue, *Thua Thien Hue Provincial Electronic Information Portal.* Accessed online at: https://hue.gov.vn/Du-dia-chi

48 Moses W J, Gitelson A A, Berdnikov S & Povazhnyy V, Estimation of chlorophyll-a concentration in case II waters using MODIS and MERIS data - Successes and challenges, *Environ Res Lett*, 4 (2009) 1-8.